

The mid-infrared AC Hall effect in optimally-doped $\text{Bi}_2\text{Sr}_2\text{CaCu}_2\text{O}_{8+\delta}$

D. C. Schmadel¹, J. J. Tu², L. B. Rigal^{1,3}, D. B. Romero³, M. Grayson^{1,5}, G. D. Gu², H. D. Drew^{1,6}

¹Department of Physics, University of Maryland, College Park, Maryland 20742

²Department of Physics, Brookhaven National Laboratory, Upton, New York 11973

³Laboratoire National des Champs Magnétiques Pulsés, Toulouse, France

⁴Laboratory for Physical Sciences, University of Maryland, College Park, Maryland 20740

⁵Walter Schottky Institut, Technische Universität München, D-85748 Garching, Germany

⁶Center of Superconductivity Research, University of Maryland, College Park, Maryland 20742

A novel heterodyne detection system determines the frequency dependence from 900 to 1100 cm^{-1} and temperature dependence from 35 to 330 K of the Hall transport in single crystal, optimally doped $\text{Bi}_2\text{Sr}_2\text{CaCu}_2\text{O}_{8+\delta}$. The results show a significant disconnect from the behavior of the Hall angle in the existing data for YBCO in the far-infrared, which indicate a negative value for the real part of the Hall angle above 250 cm^{-1} , whereas that of the current work at 1000 cm^{-1} is positive. The current work when analyzed using an extended Drude formalism results in a Hall mass comparable to the ARPES Fermi mass and a scattering rate comparable to the DC longitudinal, DC Hall, and far-infrared Hall scattering rates, which, however, are only 1/4 of the ARPES values.

While the DC and infrared conductivities reveal the overall response of a system to an electric field, the Hall effect reveals the sign of the carriers as well as some information as to the path taken by them. It essentially probes the ability of the carriers to veer or bend their course. Quantities frequently used to represent the effect are the Hall angle θ_H or the longitudinal and transverse conductivities σ_{xx} and σ_{xy} with

$$\tan \theta_H = \frac{\sigma_{xy}}{\sigma_{xx}} \quad (1)$$

These quantities are normally complex for AC results. The collection of existing measurements of the DC and AC Hall effect in high temperature superconductors has revealed a most curious behavior, whose description defies all current models, while, however, apparently falling short of suggesting a comprehensive theoretical approach on its own. Some of the difficulty of identifying patterns which can be simply expressed by means of some phenomenology arises from the fact that one is hesitant to make direct comparisons between the existing AC Hall measurements conducted on epitaxial films of YBCO with those of results of ARPES and TSM on single crystal BSCCO. The YBCO films are twinned on a micron scale and the conductivity is further complicated by the existence of chains. The mid-infrared Hall measurements reported here are the first on BSCCO single crystal and should cover some of the distance in remedying this predicament.

To appreciate the present state of the search for patterns and phenomenology consider the first of the earlier work [1-3], which to an extent indicated that $\cot \theta_H$ followed squared temperature behavior:

$$\cot \theta_H = A + B T^2 \quad (2)$$

with the A proportional to Zn doping. The seemingly profound integer 2 exponent supported the two τ model consistent with Anderson's spinon-holon theory. However, in time, from a systematic study of both single layer $\text{Bi}_2\text{Sr}_{1.6}\text{La}_{0.4}\text{CuO}_y$ and bilayer $\text{Bi}_2\text{Sr}_2\text{CaCu}_2\text{O}_y$ [4] the integer 2 became 1.78 and further, clearly dependent upon doping. The far-infrared extension to DC Hall effect explored in YBCO [5-6] suggests a different phenomenology involving a squared Lorentzian with a scattering rate proportional to temperature. This representation has since matured into a two term model [7]:

$$\tan(\theta_H) = \frac{\omega_H}{\gamma_H} + \frac{\Omega \omega_H}{\gamma_H^2}$$

where Ω is interpreted as a Fermi surface scattering derivative and γ_H is to be replaced with $\gamma_H - i \omega$ for AC while remaining proportional to temperature. This form accommodates the revised exponent of 1.78 and the Zn doping in the DC limit. This far-infrared behavior

contrasts sharply with that suggested by the mid-infrared data for YBCO [8] obtained using the different spectral lines of a CO₂ laser. When the cotangent of the Hall angle is fit to a Drude model the resulting Hall mass and the Hall scattering rate, to within the accuracy of the data, display no frequency dependence within the range from 949 to 1079 cm⁻¹. However, the Hall frequency displays a slight decrease with increasing temperature, whereas the Hall scattering rate increases linearly with temperature from near zero at T_c to over 300 cm⁻¹ at 250 K. However, the chain contribution from the epitaxially grown, twinned sample introduces considerable uncertainty in these results for the scattering rate and Hall mass.

In addition to transport results let us also consider the closely related work with Angle-Resolved Photoemission Spectra (ARPES). In the past several years ARPES has mapped the Fermi surface and identified the d-wave symmetry of the order parameter. Using $k_F = .446 \text{ \AA}^{-1}$ and $v_F = 1.8 \text{ eV \AA}$ [9,10] the ARPES Fermi surface mass is

$$m_F = \frac{\hbar k_F^*}{v_F} = \hbar k_F^* \left(\frac{1}{\hbar} \frac{\partial E}{\partial k} \right)^{-1} = 2.9 m_e$$

where $k_F^* = 0.69 \text{ \AA}^{-1}$ is the Fermi wavenumber for the hole-like surface. The quasiparticle relaxation rate Γ can be estimated from the ARPES spectral density function at the Fermi energy either directly from the EDC line widths or from the MDC line widths, Δk , as $\Gamma \approx v_F \Delta k$, where v_F is the measured Fermi velocity. The existing ARPES data on BSCCO finds that $\Gamma \propto T$. However, the minimum Γ deduced from ARPES corresponding to the (π, π) or nodal direction on the Fermi surface are four times larger than the measured IR relaxation rates. It is not known whether this discrepancy can be reconciled in terms of small angle scattering issues or Fermi liquid effects or if it requires a more exotic interpretation.

One additional feature discovered by ARPES measurements and reported by P. V. Bogdanov *et al.* [11] is a kink in the quasiparticle dispersion curve, which for Bi₂ Sr₂ CaCu₂ O₈ occurs at about 50±15 meV. The change in slope results in a reduction in velocity of around a factor of two above the kink. Z. X. Shen *et al.* [12] also report this kink occurring in LSCO at around 70 meV. The possibilities discussed for the origin of the kink are electron-phonon

interaction, the opening of a 50 meV superconducting gap, spin resonance, or some type of interaction with the theorized stripe phase. It should be noted that LSCO does not show a strong spin resonance in neutron scattering

The experimental system of the current work measures the very small complex Faraday angle imparted to CO₂ laser radiation traveling perpendicular to and transmitted by the sample immersed in a perpendicular magnetic field. The system is the same as that used by in the earlier YBCO study [8] with the addition of an inline calibration system and a continuous stress-free temperature scan provision, and further modified to place a diffraction-limited spot on the sample with post-sample spatial filtering [13].

The sample of the current work was cleaved or, rather, peeled from a single bulk crystal and placed in thermal contact with a wedged BaF crystal. Measurement of the AC magnetic susceptance measurements of this mounted peeled segment revealed a most precipitous drop with less than 1K width and a T_c of 92 K. This measurement was performed after all of the Hall measurements had been completed and therefore certainly establishes the integrity of the sample and recommend the Hall data as representative of optimally doped BSCCO. Infrared conductivity data from measurements performed on bulk crystals from the same batch supplied the real and imaginary parts of σ_{xx}. The calculation of σ_{xy} takes into consideration the multilayer reflection effects within the BSCCO film by means of the following equation, which is in CGS units

$$\sigma_{xy} = (\theta_f + i \theta_d) \frac{\omega (N)^2}{2 \pi} \frac{(n N+N) - i \tan(k d) (n+N^2)}{k d(n+N^2) - \tan(k d) [n+i k d (1+n) N-N^2]} \quad (3)$$

where θ_f and θ_d are the real and imaginary parts of the measured Faraday angle

N is the index of refraction of BSCCO determined from σ_{xx} ≈ - $\frac{i \omega}{4 \pi} N_p^2$

$k = \frac{2 \pi N}{\lambda}$ is the propagation constant in the BSCCO film,

n is the index of refraction of BaF,

ω is the radial laser frequency

and d is the thickness of the BSCCO.

To form θ_H one would usually divide σ_{xy} of Eq. (3) by the value of σ_{xx} corresponding to the same temperature and frequency. But here, we wish to examine that part of the Hall angle related to the "free carriers." Interband transitions, which are on the order of ~ 1 volt, contribute essentially nothing to σ_{xy} . However, we must remove their somewhat more substantial contribution to σ_{xx} before taking the ratio. In CGS units

$$\begin{aligned}\epsilon_{\text{total}} &= \epsilon_{\text{bound}} + i \frac{4 \pi \sigma_{\text{free}}}{\omega} \\ &= i \frac{4 \pi \sigma_{\text{total}}}{\omega}\end{aligned}$$

Therefore,

$$\sigma_{\text{free}} = \left(\sigma_{\text{total}} + \frac{i \omega \epsilon_{\text{bound}}}{4 \pi} \right) \quad \text{CGS} \quad (4)$$

For ϵ_{bound} we use the value $\epsilon_{\infty} = 4.6$ from Quijada [14]. For σ_{total} we use σ_{xx} determined from reflectance measurements performed on crystals from the same batch. The sample thickness was determined by transmission measurements on the peeled sample.

Figure 1 displays the resulting values of θ_H versus frequency. Clearly, both real and imaginary parts are decreasing with frequency. Here, we are fascinated with a nearly Drude behavior for both real and imaginary parts. The imaginary part displays much less frequency dependence than the real part. Its average value is approximately twice that of the real part. Recall that for a Drude model the phase of the Hall angle (the ratio of the imaginary to the real part) equals ω/γ . We shall see below that this is in agreement with the scattering rate of 500 cm^{-1} at 300 K , which results when the data is analyzed as a Drude form. Figure 2 displays the values of θ_H versus temperature. The real part of θ_H increases with temperature but appears to saturate around 300 K . Note that the real part of the Hall angle is positive for all temperatures in the normal state. The imaginary part of the Hall angle is decreasing with temperature in a very linear fashion.

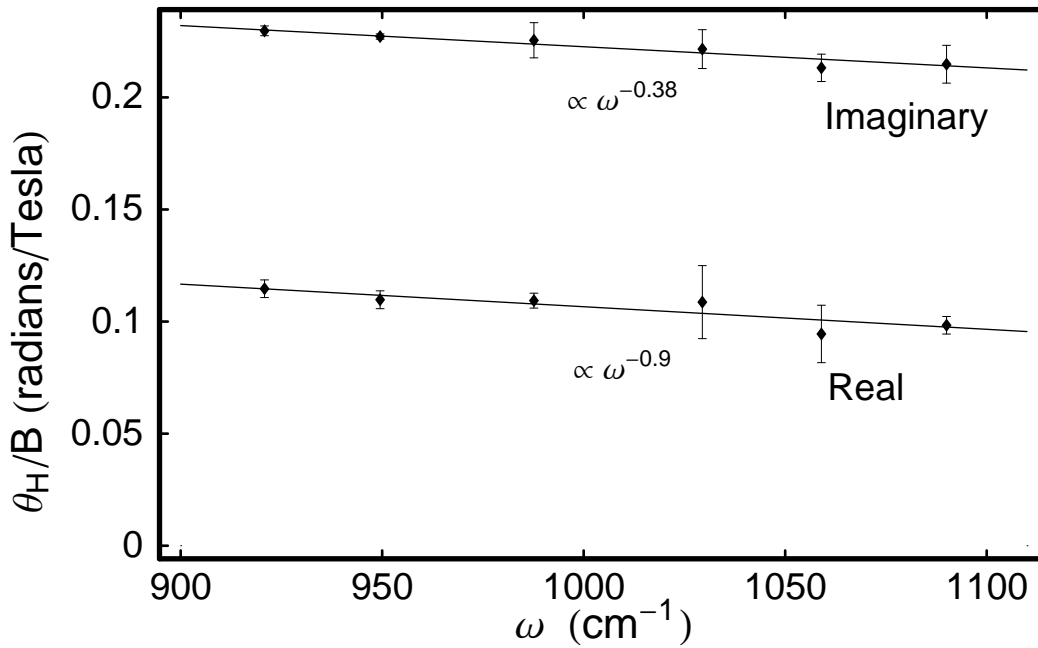


FIG. 1 The real and imaginary parts of θ_H / Tesla for 2212 BSCCO, versus frequency along with linear fits.

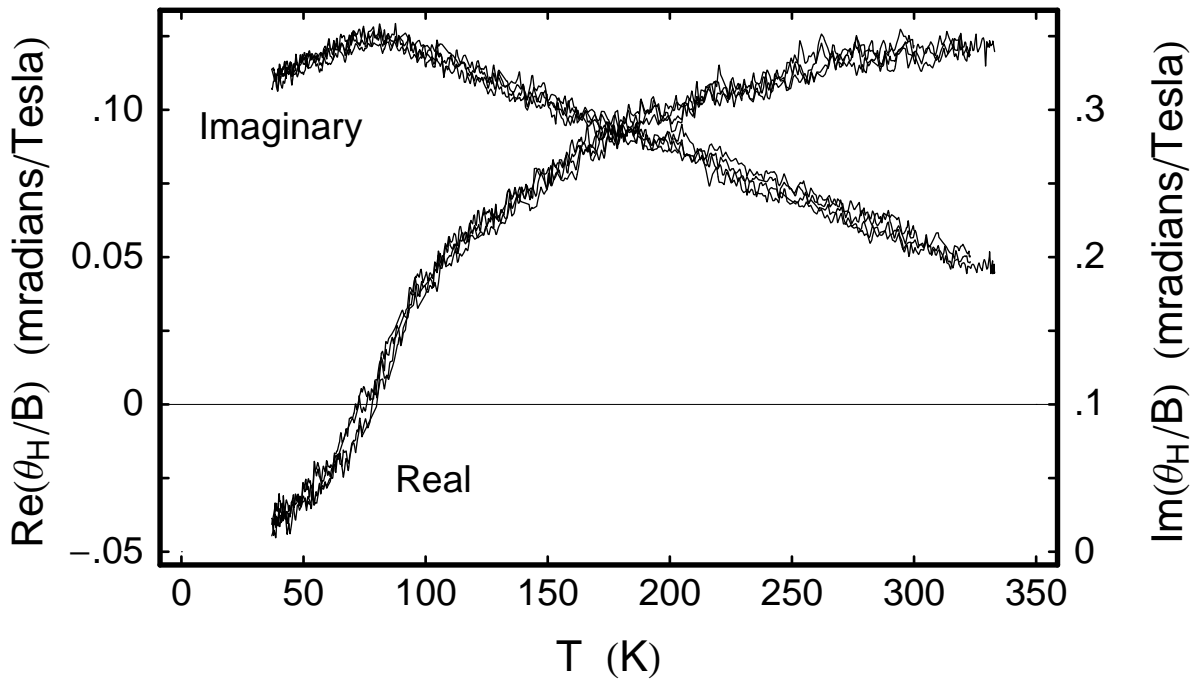


FIG. 2 The real and imaginary parts of θ_H / Tesla versus temperature for 2212 BSCCO.

Figure 3 compares the real part of the Hall angle with that from the far-infrared data [6]. We observe a disconnect between the behavior of the far- and mid-infrared Hall angle. Starting at about 230 cm^{-1} the real part of the Hall angle for low temperatures appears to be negative. However, as noted above it is certainly positive in the mid-infrared. The temperature dependence of the far-infrared data changes sign at around 150 cm^{-1} , which then agrees with that of the mid-infrared. The thin lines are fits of squared Lorentzians, which accommodate the far-infrared results well. However, the extension of the real part into the mid-infrared remains negative unlike the data which are positive. There are innumerable ways to accommodate this plunge in the real part of the Hall angle at 300 cm^{-1} and to join these results with those of the mid-infrared of the current work. All would require at least one minimum and at least one maximum between 300 to perhaps 600 cm^{-1} as might be caused by a resonance. However, though no such feature is seen in the data for σ_{xx} [15], a peak is present at $\sim 300 \text{ cm}^{-1}$ in the phase of σ_{xx} in the plot of $\text{Im } \sigma_{xx} / \text{Re } \sigma_{xx}$ at 100 K shown in Fig. XXX. It is interesting to note that this feature in the phase is not predicted by the coldspot model [16]. Further, its frequency roughly corresponds to numerous other phenomena including the 41 meV spin resonance, the 50 ± 15 meV phonon interaction [11], the superconducting gap, and the quasiparticle band width of the three band Hubbard model.

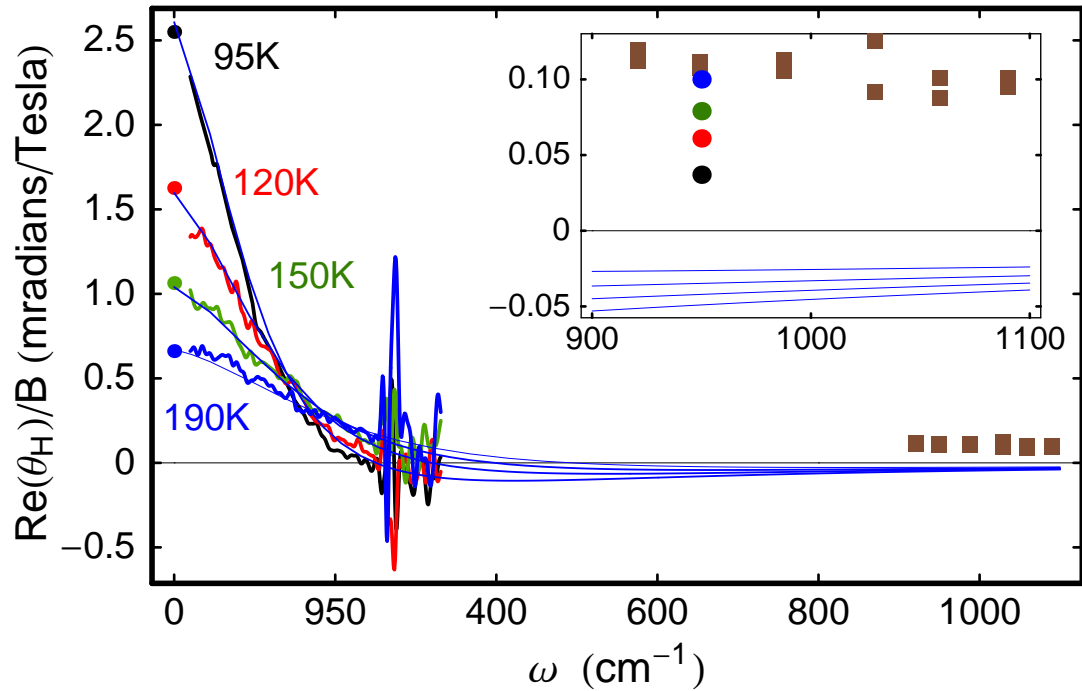


FIG. 3 The real and imaginary parts of θ_H /Tesla versus temperature for 2212 BSCCO. The mid-infrared data is shown in the inset with expanded axes. The brown points in the inset correspond to 300 K. The other colors of the points at 950 cm^{-1} within the inset correspond to the same temperatures as in the main plot.

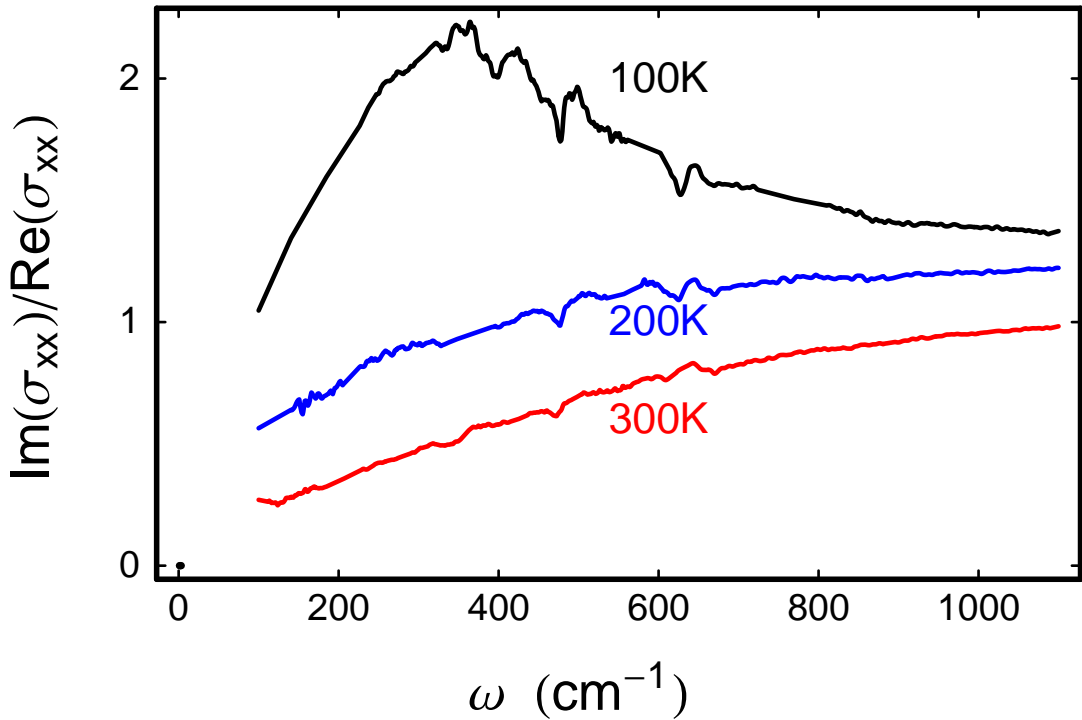


FIG. 3 $\text{Im } \sigma_{\text{xx}} / \text{Re } \sigma_{\text{xx}}$ vs. frequency for single crystal 2212 BSCCO.

We now apply the extended Drude formalism to the data of the current work. Much effort has been expended to explain the earlier apparent T^2 behavior of the cotangent of the DC Hall angle. This was thought to arise out of a T^2 dependence of a Hall scattering rate. However, both the current mid-infrared results and the squared Lorentzian analysis of the far-infrared Hall data [6] suggest that the characteristic behavior of scattering in the cuprates is a linear increase with temperature through a squared Lorentzian. However, the features, which in the far-infrared conduced to the squared Lorentzian form, are not present in the mid-infrared. For example, the extended Drude analysis reveals a mid-infrared scattering rate increasing slowly with frequency, whereas that of the far-infrared decreases with frequency even perhaps becoming negative above 250 cm^{-1} .

The linear temperature dependence of the Hall scattering rate in the mid-infrared also disagrees with the ARPES results for $-\text{Im}\Sigma$ [10], which imply a decreasing temperature dependence with increasing frequency as is also seen in σ_{xx} . Even marginal Fermi liquid theory, which favors a linear temperature dependence of the scattering is at odds with the lack

of frequency dependence. Recall that a frequency dependence would have caused a significant positive intercept in the zero temperature projection of the normal state scattering rate in Fig. 4. The lack of frequency dependence of the scattering rate of the current work on the other hand contravenes both Fermi liquid and marginal Fermi liquid theories, which claim a strong frequency dependence for the scattering rate at temperatures low compared to the energies corresponding to the frequencies. In the present circumstance

$\omega = 1000 \approx 125 \text{ meV} > k_B 300 \text{ K} \approx 25 \text{ meV}$, yet there is little to no frequency dependence of the scattering rate. The far-infrared scattering rate when compared to that of the mid-infrared curiously exhibits the same linear increase with temperature. However, the projection of the normal state mid-infrared scattering rate to zero temperature is negative. This feature was also observed for YBCO [8].

Figure 4 also shows the scattering rates corresponding to other measured quantities including γ^* extrapolated to dc for BSCCO [15] determined from inverse of the slope approaching zero frequency in Fig. 3:

$$\gamma^* = \frac{\gamma}{1+\gamma(\omega)} = -\omega \frac{\text{Re}(1/\sigma)}{\text{Im}(1/\sigma)} = \omega \frac{\text{Re}(\sigma)}{\text{Im}(\sigma)}$$

Additionally the figure displays σ_{xx} for YBCO at DC designated "Quijada γ^* " [14], θ_H for YBCO at DC and far-infrared using the squared Lorentzian analysis designated "Grayson γ_H^2 " and for a simple Drude applied to σ_{xy} designated "Grayson γ_{xy} " [6], θ_H for BSCCO at 0.2–1.0 THz designated "Corson γ^* " [17], θ_H for YBCO at 1000cm^{-1} designated "Rigal γ_H " [18], and the ARPES zero frequency value for Γ designated "Valla Γ " [9]. Remarkably at moderate temperatures all but the ARPES scattering rates agree. This suggests the existence of a universal transport scattering rate for the DC longitudinal conductivity which for Hall conduction is nearly independent of frequency. Curiously this scattering rate is not shared by ARPES.

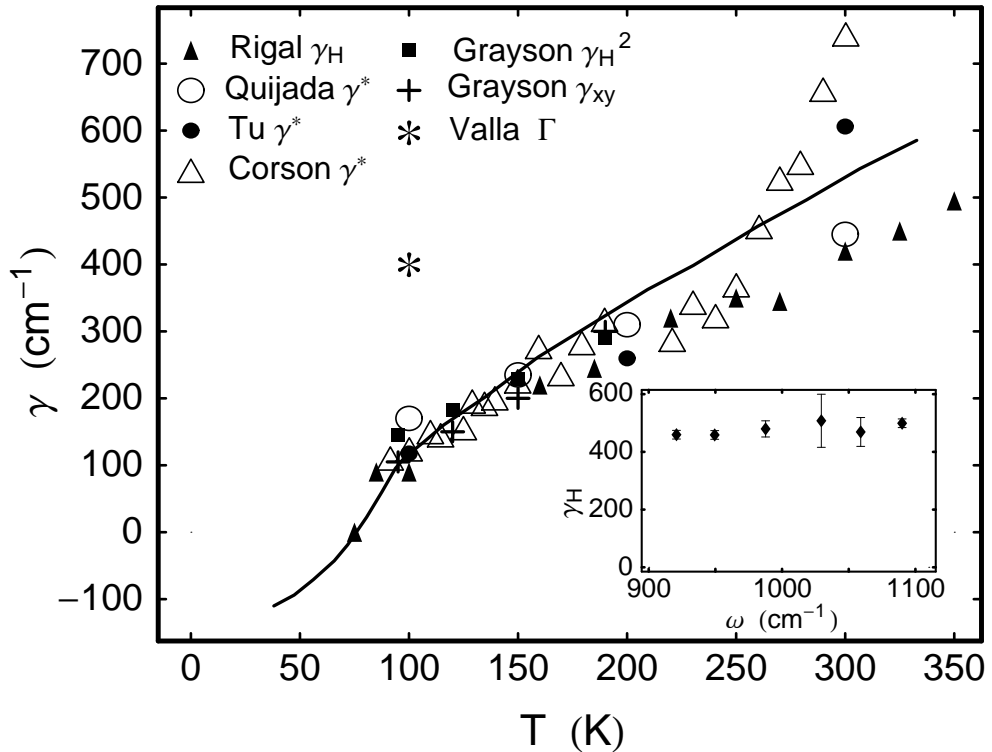


FIG. 4 Various scattering rates versus temperature. The thick black line demonstrates the frequency dependence of the Hall scattering rate in the mid-infrared region. The mid-infrared scattering rate is also shown in the inset versus frequency.

Figure 5 displays the Hall mass, which is roughly twice the value of the longitudinal mass calculated from σ_{xx} in the mid-infrared. The frequency dependences for the Hall mass and longitudinal mass are similar displaying a slow decrease with increasing frequency. However, the temperature dependences of the masses are opposite each other with the Hall mass actually increasing about 20% over the temperature range of 100 to 300K. Furthermore, the extended Drude analysis of the far-infrared Hall data [6], suggest a mass enhancement with a full linear temperature dependence actually doubling from 95K to 190K and also increasing with frequency. Finally, the same ARPES measurements which imply a very different scattering rate return to identify a full dressed mass which is nearly equal to the calculated mid-infrared Hall mass.

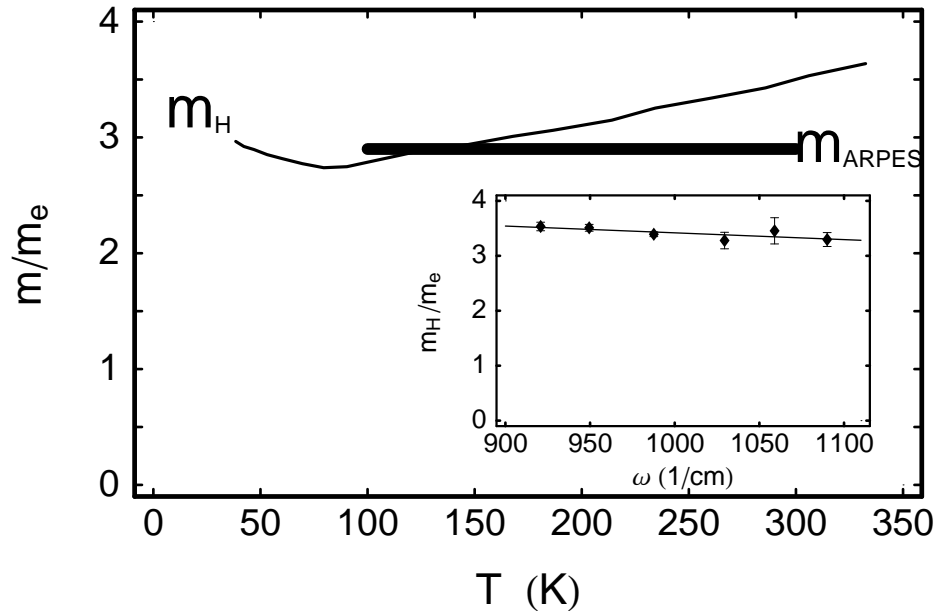


FIG. 5 The mid-infrared Hall mass (thin line) and the ARPES Fermi surface mass (thick line) both versus temperature. The mid-infrared Hall mass is also shown in the inset versus frequency.

REFERENCES

¹N. P. Ong, *et al.*, Phys. Rev. B **35**, 8807(1987).

²T. R. Chien, Z. Z. Wang, and N. P. Ong, Phys. Rev. Lett. **67**, 2088(1991).

³J. M. Harris, Y. F. Yan, and N.P. Ong, Phys. Rev, B **46**, 14293 (1992).

⁴Z. Konstantinovic, Z. Z. Li, and H. Raffy, Phys. Rev. B **62**, 11989(2000).

⁵S, G, Kaplan *et al.*, Phys. Rev. Lett. **76**, 696 (1996).

⁶M. Grayson, L. B. Rigal, D. C. Schmadel, H. D. Drew, and P. J. Kung, Phys. Rev. Lett. **89**, 037003 (2002).

⁷M. Grayson, H. D. Drew Trieste poster (unpublished)

⁸J. Cerne *et al.*, Phys. Rev. Lett. **84**, 3418 (2000).

⁹T. Valla *et al.*, Phys. Rev. Lett. **85**, 828 (2000).

¹⁰T. Valla *et al.*, Science **285**, 2110 (1999).

¹¹P. V. Bodanov *et al.*, Phys. Rev. Lett. **85**, 2581 (2000).

¹²Z. X. Shen *et al.*, arXiv:cond–mat/0108381(2001)(unpublished).

¹³J. Cerne *et al.*, cond–mat/xxxxx(2002)(unpublished).

¹⁴M. A. Quijada, Ph.D. thesis, University of Florida, 1994.

¹⁵J. J. Tu *et al.*, Phys. Rev. B (in press) (2002)

¹⁶L. B. Ioffe and A. J. Millis, Phys. Rev. B **58**, 11631 (1998)

¹⁷J. Corson, J. Orenstein, Seongshik Oh, J. O'Donnell, J. N. Eckstein, cond–mat/0006027(2000)(unpublished).

¹⁸L. B. Rigal (unpublished data).